Geometric Design of Three-Phalanx Underactuated Fingers

Lionel Birglen and Clément M. Gosselin

Department of Mechanical Engineering, Laval University, Québec, QC, G1K 7P4, Canada
Tel: (418) 656-3474, Fax: (418) 656-7415,
email: birgle00@gmc.ulaval.ca, gosselin@gmc.ulaval.ca

Abstract

This paper studies the grasp stability of two classes of three-phalanx underactuated fingers with transmission mechanisms based on either linkages or tendons and pulleys. The concept of underactuation in robotic fingers—with fewer actuators than degrees of freedom (DOF)—allows the hand to adjust itself to an irregularly shaped object without complex control strategy and sensors. With a n-phalanx finger, n contacts (one for each phalanx) are normally required to statically constrain the finger. However, some contact forces may be lacking due to either the transmission mechanism, or simply the object size and position. Thus, one may define an i^{th} order equilibrium, when the finger is in static equilibrium with i missing contacts. In this paper, the case for which $n = 3$ is studied with a particular emphasis on the cases for which $i = 1$ and $i = 2$. The fact that some contact forces do not appear or are negative, can lead in some cases to the ejection of the object from the hand, when no equilibrium configuration is achieved.

1 Introduction

Until now, the human hand remains unmatched despite numerous and interesting attempts to copy the latter. Pioneer designs include: the Utah/MIT hand [1], the Stanford/JPL (Salisbury's) hand [2], the hands from the DLR [3], the Okada hand [4], and many others. However, significant efforts have been made to find designs that are simple enough to be easily built and controlled in order to obtain practical systems [5]. To this end, a particular emphasis has been placed on the reduction of the number of degrees of freedom, thereby decreasing the number of actuators. In particular, the SSL hand [6], the DIES-DIEM hand [7], and the Cassino finger [8] have followed this path. On the other hand, few prototypes involve a smaller number of actuators without decreasing the number of degrees of freedom.This approach, referred to as *underactuation* can be implemented through the use of passive elements like mechanical limits or springs leading to a mechanical adaptation of the finger to the shape of the object to be grasped [9–13]. An illustration of the closing sequence of a two-phalanx underactuated finger is presented in Fig. 1 in order to clearly illustrate the concept of underactuation. The finger is actuated through the lower link, as shown by the arrow. Since there are two phalanges and one actuator, one (two minus one) elastic element is used to constrain the finger. In this example, an extension spring tends to maintain the finger fully extended and in contact with a mechanical limit. First, the finger behaves as a single rigid body in rotation about the base pivot. Then, the proximal phalanx makes contact with the object, the actuation torque overcomes the spring preloading and the distal phalanx begins to rotate. Finally, both phalanges are in contact with the object and the finger has completed the shape adaptation phase, the actuator force is distributed among the two phalanges in contact with the object. It should be noted that this closing sequence occurs with a continuous motion of the actuator and without feedback.

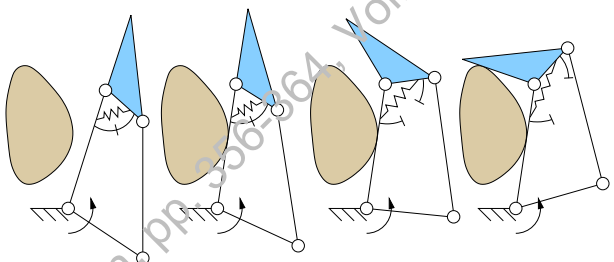

Fig. 1: Two-phalanx underactuated finger: closing sequence.

This technique can be generalized to any number of phalanges, and in this paper, the three-phalanx case is considered. Previously, significant progress has been achieved by intuitive designs from outstanding individuals, to create underactuated fingers. However, this method may overlook theoretical issues and it is the purpose of this paper to establish the foundations of a theoretical background to study the grasp stability of such fingers. Biomimetic approaches have been used in the past and are usually reliable since they rely on the results on the natural selection. However, understanding the qualities and drawbacks of these designs can help to overcome their limits. One should also keep in mind that designing a robot is not the same as producing robust living creatures, with distinct constraints and different objectives. In [14] and [15], the fact that underactuated fingers cannot always apply forces with all their phalanges in all configurations was presented and the consequences were discussed. In fact, even if a fully positive workspace is provided, i.e. with a finger that can always provide positive contact forces with all its phalanges, one cannot guarantee that contact between the object and the finger will be made with all the phalanges, depending on the object size and position. Therefore, the mobility of a n-phalanx underactuated finger with less-than-n contacts should be studied. In this paper, the case for which $n = 3$ is presented and a technique to study the grasp stability is introduced.

2 Force Properties of Underactuated Fingers

2.1 Introduction Underactuation in robotic hands leads to intriguing properties that have never been fully studied. An

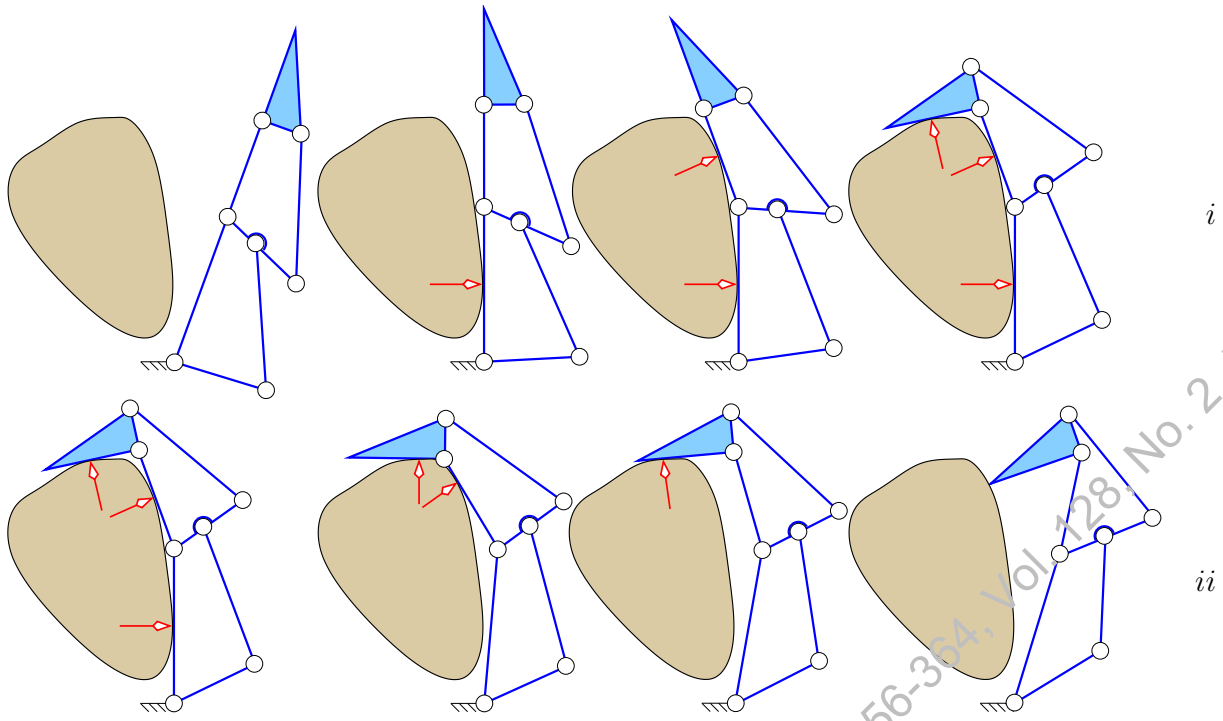

Fig. 2: Ideal grasping sequence (i) degenerating into ejection (ii).

ideal grasping sequence as illustrated in Figs. 1 and 2i might not always occur. Indeed, in the final configuration (a configuration is defined as the set of finger joint angles and the contact locations), some phalanx forces may be negative. Note that in both cases and also in the whole paper, the object seized is assumed fixed in space. With this hypothesis, multiple finger grasps can be reduced to single finger grasps and analyzed using the method presented in the paper. If one or more phalanx force is negative, the corresponding phalanx will loose contact with the object. Then, another step in the grasping process will take place: the remaining phalanges corresponding to positive forces will slide on the object surface. The reason of this sliding motion is that the finger in its original configuration cannot be in static equilibrium, because the latter would require negative contact forces. The sliding process will continue until either a stable configuration is achieved (with only positive or zero phalanx forces), or joint limits are met (a stable situation, but the shape adaptation is less effective), or the last phalanx will curl away and loose contact with the object (the ejection phenomenon, illustrated in Fig. 2ii). Indeed, to constrain a n-phalanx finger, n contacts are usually required. However, $n-i$ contacts can be enough for the finger to be in static equilibrium, if certain geometric conditions are met. Thus, one can describe an i^{th} order equilibrium when i contacts are lacking. In this paper, the case for which $n=3$ is studied and a particular emphasis is placed on the case for which $i=1$. A discussion will be presented for $i=2$, while the case $i=0$ has been presented in [15]. In this work, a stable grasp means that the finger is in static equilibrium. The occurrence of the situations where one (or more) phalanx force is negative should be decreased (prevention may be impossible) and ejection avoided. Thus, some fundamental questions should be answered: "how can we guarantee that a grasp is stable" and its direct corollary: "how can we increase the occurrence of these stable situations." These questions and their answers allow one to obtain optimally stable fingers. To this end, the results of the grasp stability theory for two-phalanx underactuated fingers are first briefly recalled.

2.2 On the two-phalanx underactuated finger ejection theory In order to determine the configurations where a two-phalanx underactuated finger can apply forces to the object grasped, a quasi-static model was developed [15]. The models of fingers used are depicted in Fig. 3. The following expressions were obtained:

$$f_1 = \left[\frac{k_2(1+R)+Rl_1\cos\theta_2}{k_1k_2}\right]T_a \quad \text{and} \quad f_2 = -\frac{RT_a}{k_2} \qquad (1)$$

where $\mathbf{f} = [f_1\ f_2]^T$ is the vector of normal contact forces vector, i.e. f_1 and f_2 are respectively the proximal and distal phalanx normal forces, k_1 and k_2 are the contact locations on their respective phalanges, θ_2 is the angle between the phalanges and finally R is the transmission factor [15] characterizing the mechanism used to transmit the actuation torque T_a to the phalanges. This factor can depend on the angle θ_2 (e.g. for linkage-driven fingers) or be constant (e.g. for tendon-driven fingers). When f_1 is negative, the proximal phalanx contact is lost and the distal phalanx slides on the object until either a stable grasp (static equilibrium) is achieved or ejection occurs ($k_2 > l_2$). The distal phalanx contact is lost only in rare singular cases corresponding to hyperflexion/hyperextension of the finger in the case of a linkage transmission and never with tendon-driven fingers, hence this case will be dismissed. Depending on the the pair (k_2, θ_2), one can obtain the final stability of the grasp depending on an initial contact situation.

It has been shown [15] that the grasp stability does not depend on k_1 or θ_1. An example of the grasp-state plane described by (k_2, θ_2) and depicting the grasp stability corresponding to this sliding motion of the distal phalanx is presented in Fig. 4. The contact trajectories, indicated by dotted curves in Fig. 4, are defined by

$$k_2^2 - k_{2i}^2 + 2l_1(k_2 \cos\theta_2 - k_{2i} \cos\theta_{2i}) = 0. \qquad (2)$$

where k_{2i} and θ_{2i} are an arbitrary initial configuration. Each of these contact trajectories corresponds to a different contact point in space, i.e. different k_{2i} and θ_{2i}, and the sliding motion takes place around this contact point. Eq. (2) allows to obtain the precise evolution of the contact position with respect to the evolution of θ_2. The contact situation (k_2, θ_2) during the sliding evolves along one of these contact trajectories until either attaining a stable situation (the curves labeled "Equilibrium location") or physically leaving the distal phalanx ($k_2 > l_2$, ejection). More details on this plane and its characteristic elements like the equilibrium curve can be found in [14].

For instance, if the initial contact is established in configuration A (indicated in Fig. 4), the two-phalanx contact configuration is unstable (the proximal force is negative). Then, contact with the proximal phalanx is lost and the finger undergoes a sliding motion described by the associated contact trajectory until, in this case, configuration B where the finger is in static equilibrium. On the other hand, if the initial contact is in configuration C, once again the proximal force is negative and its associated contact lost, but in this case, the sliding motion continues until configuration D where the distal contact is also lost and the finger ejects the object.

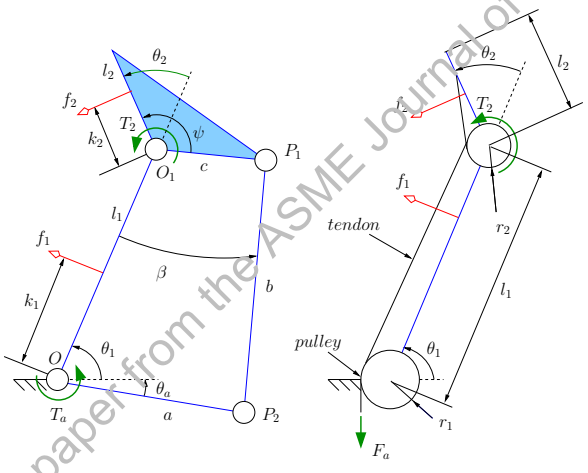

Fig. 3: Two-phalanx fingers.

Two types of ejections were defined according to the motion of the distal phalanx: opening- and closing-ejection. A necessary and sufficient condition to eliminate opening ejection was to use mechanical limits on angle θ_2 such that $0 < \theta_2 < \pi/2$ [16]. Closing-ejection can be eliminated using different solutions [16].

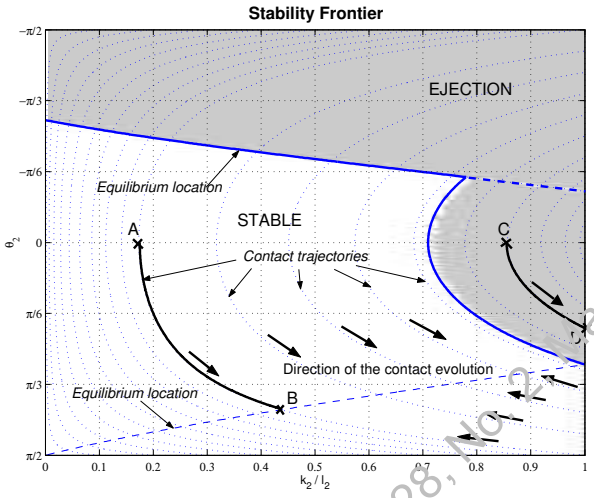

Fig. 4: Final stability of the grasp with one phalanx contact.

3 On the three-phalanx underactuated finger ejection theory

The objective of this work is to determine when a grasp is stable and if ejection can occur with a three-phalanx finger. Preliminary experiments with *ADAMS*, a commercial dynamic simulation package, suggest that, indeed, ejection can happen with a three-phalanx underactuated finger. However, such conditions do not occur very often and they are very likely favoured by particular conditions of the model used (e.g. single-point contacts, no friction). In this paper, it is assumed that the initial configuration of the finger is the one depicted in the last schematic of the ideal grasping sequence (Fig. 2*i*). Thereupon, in this configuration, some forces may be negative. The case where the three forces are negative is not very likely to happen, in fact with a tendon-driven underactuated finger, it is even impossible since the last phalanx force is *always* positive [15]. Furthermore, it contradicts the closing motion of the finger necessary to achieve the initial configuration. For linkage-driven fingers, particular configurations of the transmission linkages can correspond to a negative or zero distal phalanx force. These configurations correspond to hyperflexion/hyperextension in the finger or singularity in the transmission linkages. They have been studied in [15]. These situations will not be represented in the forthcoming figures for legibility purposes but should be taken into account.

Geometric details and nomenclature of the two models considered in this paper are provided in Figs. 5 and 6. The equivalence between linkages and tendon transmissions has been highlighted in [15], both types of transmission share similar properties. Numerical results and figures will be given for fingers with the geometric parameters listed in Table 1.
If only one contact force is negative, the interesting cases reduce to only three, which are presented in Fig. 7. The equilibrium is achieved when the force on the phalanx with no contact (the initially negative force) increases to zero, while the others remain positive. The procedure to obtain an analytical expression of the normal contact forces has

Table 1: *Geometric parameters*

Set 1 (linkages)									
l_1	l_2	l_3	ψ	a_1	b_1	c_1	a_2	b_2	c_2
1	.67	.62	$\pi/2$	.62	.95	.26	.62	.95	.26
Set 2 (pulleys)									
l_1	l_2	l_3	–	r_1	–	r_2	r_3	–	r_4
1	.67	.62	–	.62	–	.26	.62	–	.26

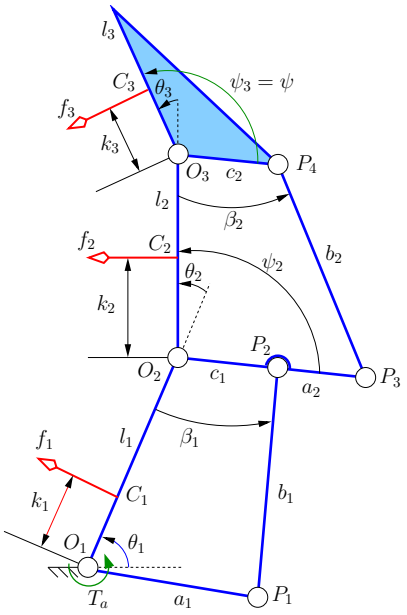

Fig. 5: Three-phalanx finger using linkages (springs not indicated for legibility purposes).

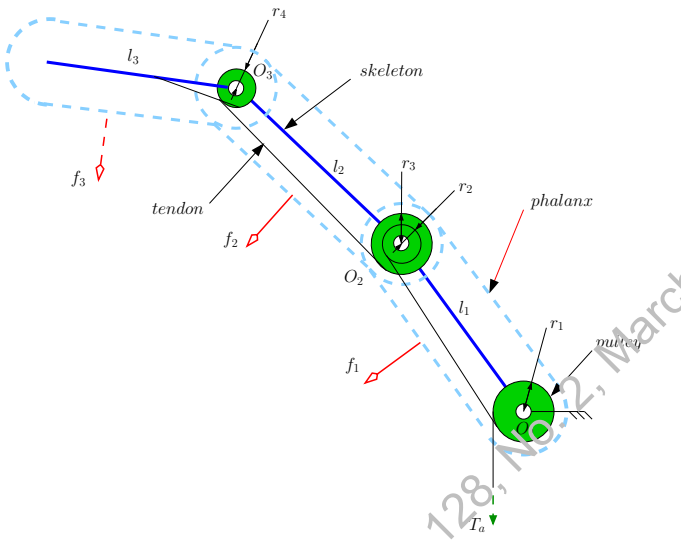

Fig. 6: Three-phalanx finger using tendons (springs not indicated for legibility purposes).

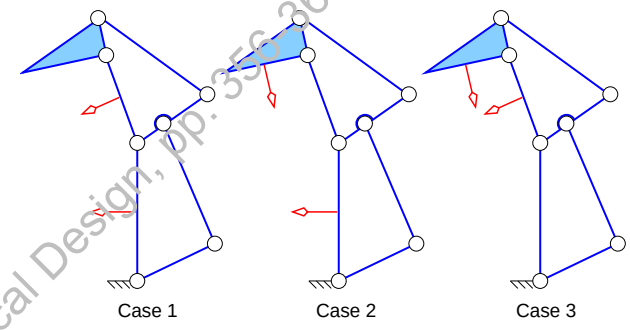

Fig. 7: Cases studied for ejection.

been presented in [15]. Basically, the contact forces can be expressed as:

$$\mathbf{f} = \mathbf{J}^{-T}\mathbf{T}^{-T}\mathbf{t} \tag{3}$$

where $\mathbf{f} = [f_1\ f_2\ f_3]^T$ is the vector of the normal contact forces and $\mathbf{t}$ is the input torque vector exerted by the actuator and the springs, i.e. $\mathbf{t} = [T_a\ T_2\ T_3]^T$. Matrix $\mathbf{J}$ is a lower triangular matrix characteristic of the contact locations (and friction, if modeled) that can be expressed analytically [15]. Neglecting friction, one has:

$$\mathbf{J} = \begin{bmatrix} k_1 & 0 & 0 \\ k_2 + l_1 C_{\theta_2} & k_2 & 0 \\ k_3 + l_1 C_{\theta_2+\theta_3} + l_2 C_{\theta_3} & k_3 + l_2 C_{\theta_3} & k_3 \end{bmatrix}, \tag{4}$$

where $C_\alpha = \cos\alpha$, symbols are indicated in Fig. 5. It is observed that this matrix can also be used with fully-actuated fingers. Matrix $\mathbf{T}$ is characteristic of underactuation (it becomes the identity matrix for fully-actuated fingers) and, more precisely, of the transmission mechanism used. For a finger using linkages as illustrated in Fig. 5, one has:

$$\mathbf{T} = \begin{bmatrix} 1 & -\frac{h_2}{h_2+l_1} & -\frac{h_2 h_3}{(h_2+l_1)(h_3+l_2)} \\ 0 & 1 & 0 \\ 0 & 0 & 1 \end{bmatrix}, \tag{5}$$

where

$$h_i = c_{i-1}\left(\cos(\theta_i - \psi_i) - \sin(\theta_i - \psi_i)\cot\beta_{i-1}\right) \tag{6}$$

is the signed distance between point O_i and the geometric intersection of lines $(O_{i-1}O_i)$ and $(P_{2i-2}P_{2i-3})$. This value can be negative if the intersection point is on the same side as O_{i-1} with respect to O_i. Angle ψ_i is the angle between O_iP_{2i-2} and O_iO_{i+1} for $i > 1$, i.e.

$$\begin{aligned} \psi_i \quad = \quad & \text{atan}\left[\frac{-c_i \sin(\theta_{i+1}-\psi_{i+1})}{l_i + c_i\cos(\theta_{i+1}-\psi_{i+1})}\right] \\ & + \text{acos}\left[\frac{l_i^2 + a_i^2 + c_i^2 - b_i^2 + 2c_i l_i \cos(\theta_{i+1}-\psi_{i+1})}{2a_i\sqrt{c_i^2 + 2c_i l_i \cos(\theta_{i+1}-\psi_{i+1}) + l_i^2}}\right] \end{aligned} \tag{7}$$

Thus, angle ψ_i can be expressed recursively with, initially, $\psi_3 = \psi$. For tendon-driven fingers, the expressions are simpler, i.e. one has

$$\mathbf{T} = \begin{bmatrix} 1 & -\frac{r_2}{r_1} & -\frac{r_2 r_4}{r_1 r_3} \\ 0 & 1 & 0 \\ 0 & 0 & 1 \end{bmatrix} \tag{8}$$

where r_{2i-1} and r_{2i} for $i > 0$ are respectively the radius of the pulley located at the base and at the end of the i^{th} phalanx (cf. Fig. 6).

Hence, the expressions of the contact forces are

$$f_1 = \frac{l_1 U T_a}{k_1 k_2 k_3 (h_2 + l_1)(h_3 + l_2)} \tag{9}$$

$$f_2 = \frac{h_2 l_2 (k_3 - h_3 \cos\theta_3) T_a}{k_2 k_3 (h_2 + l_1)(h_3 + l_2)} \tag{10}$$

$$f_3 = \frac{h_2 h_3 T_a}{k_3 (h_2 + l_1)(h_3 + l_2)} \tag{11}$$

with

$$\begin{aligned} U = \quad & k_2 k_3 h_3 + k_2 k_3 l_2 - h_2 k_3 l_2 \cos\theta_2 \\ & + h_2 h_3 l_2 \cos\theta_2 \cos\theta_3 - h_2 h_3 k_2 \cos(\theta_2 + \theta_3) \end{aligned} \tag{12}$$

for a linkage-driven finger, and

$$f_1 = \frac{U' T_a}{k_1 k_2 k_3 r_1 r_3} \tag{13}$$

$$f_2 = \frac{-r_2(-k_3 r_3 + r_4 l_2 \cos\theta_3 + r_4 k_3) T_a}{k_2 k_3 r_1 r_3} \tag{14}$$

$$f_3 = \frac{r_2 r_4 T_a}{r_1 r_3 k_3} \tag{15}$$

with

$$\begin{aligned} U' = {} & l_1 r_2 \cos\theta_2 (r_4 l_2 \cos\theta_3 + (r_4 - r_3) k_3) + \\ & k_2 k_3 r_3 (r_1 - r_2) - l_1 r_2 r_4 k_2 \cos(\theta_2 + \theta_3) \end{aligned} \tag{16}$$

for a tendon-driven finger. In the next sections, some assumptions are made on the finger architecture and the contact, namely negligible friction at the contacts and negligible spring torques between the phalanges (the latter assumptions correspond to the above expressions for the contact forces). The object will be assumed fixed with respect to the base of the finger and the local geometry of the contacts will also be neglected, i.e. a single fixed point of contact for each phalanx is assumed.

3.1 Loss of one contact

Case 1 The first case in Fig. 7 is trivial, since the distal phalanx force is always positive except in rare hyperflexion/hyperextension configurations with mechanical transmissions and never with pulleys and tendons. Therefore, an equilibrium can be attained with the contact situation of Case 1 only in such hyperflexion/hyperextension configurations, such as the one illustrated in Fig. 8. In this case, the equilibrium is achieved while the last phalanx does not touch the object. This should be prevented as the finger may not be considered to sufficiently envelope the object for proper grasping. Indeed, in this case, the finger act as if it had only two phalanges, the last one remaining unused. Design rules of four-bar linkages should be used to prevent this situation from happening.

Case 2 In the second case of Fig. 7, the finger can be regarded as a two-phalanx finger. Indeed, if contact is made and maintained with the first phalanx, the resulting configuration (with no second phalanx contact) can be considered exactly like the two-phalanx finger during a sliding motion

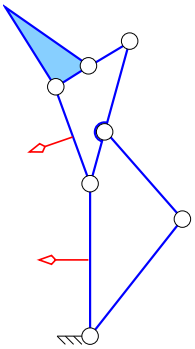

Fig. 8: Equilibrium configuration with no contact on the distal phalanx.

of the distal phalanx as introduced in Section 2.2 and studied in [14], the last two phalanges constituting a two-phalanx finger. However, the contact trajectories should be examined in the $(\theta_2, \theta_3, k_3)$ space rather than just the two-phalanx grasp-state plane (θ_3, k_3) since the angle θ_2 is required to establish the expression of the equilibrium surface described by $f_2 = 0$ as established in eq. (10) in case of a linkage-driven finger (h_2 is function of θ_2). Furthermore, this angle could be required to establish the contact forces during the sliding process, as will be discussed in Section 3.3. In the grasp-state space described by $(\theta_2, \theta_3, k_3)$, one obtains the equilibrium surface, mathematically defined by $f_2(\theta_2, \theta_3, k_3) = 0$. The plane $k_3 = l_3$ corresponds to the ejection limit illustrated in Fig. 2*ii*, if $k_3 > l_3$ contact with the distal phalanx is lost. The contact trajectories describing the instantaneous grasp-state evolution of the finger, modified from [14] to include the variation of θ_2, are

$$k_{3i} C_{\theta_{3i}} - k_3 C_{\theta_3} = K \tag{17}$$

$$l_2(1 - C_{\theta_{2i} - \theta_2}) + k_{3i}(C_{\theta_{3i}} - C_{\theta_2 - \theta_{2i} - \theta_{3i}}) = K \tag{18}$$

with

$$K = \frac{k_3^2 - k_{3i}^2}{2 l_2} \tag{19}$$

obtained by expressing that the contact location is fixed in space (the law of cosines in the triangle $O_2 O_3 C_3$) and where $(\theta_{2i}, \theta_{3i}, k_{3i})$ is an arbitrary initial contact situation on the trajectory. Eqs. (17) and (18) mathematically imply a skewing of the trajectory plotted in Fig. 4 out of the (θ_3, k_3) plane, corresponding to the variation of θ_2. Examples of contact trajectories with the associated equilibrium surfaces are presented in Figs. 9 and 10.

Once in an initial configuration, the grasp-state evolves following the trajectory until either a joint limit is attained (which can be represented by vertical planes in this space), or the equilibrium surface is attained, or ejection happens (top of the space represented, defined by $k_3 = l_3$). Note that the direction in which the instantaneous contact state evolves along the trajectory depends on the side of the equilibrium surface on which this state is located, i.e. the sign of f_2, similarly to the two-phalanx finger [14].

Hence, one obtains contact trajectories that can lead either to a static ($f_2(\theta_2, \theta_3, k_3) = 0$) or kinematic (joint limit) equilib-

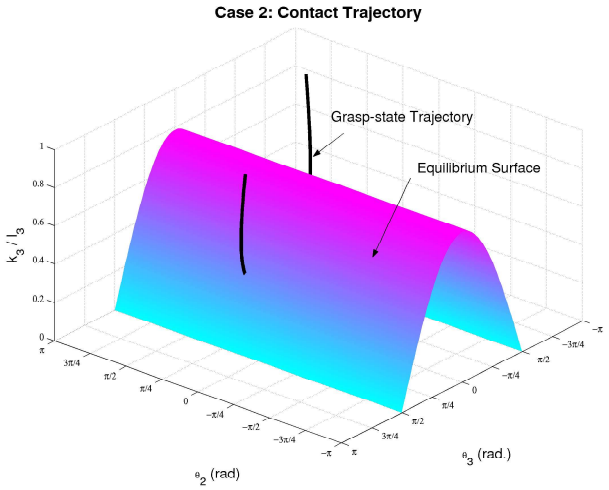

Fig. 9: Grasp-state trajectory and equilibrium surface for initial configuration $(\theta_{2i}, \theta_{3i}, k_{3i}) = (\pi/4, \pi/4, 0.16)$ - parameter set 2.

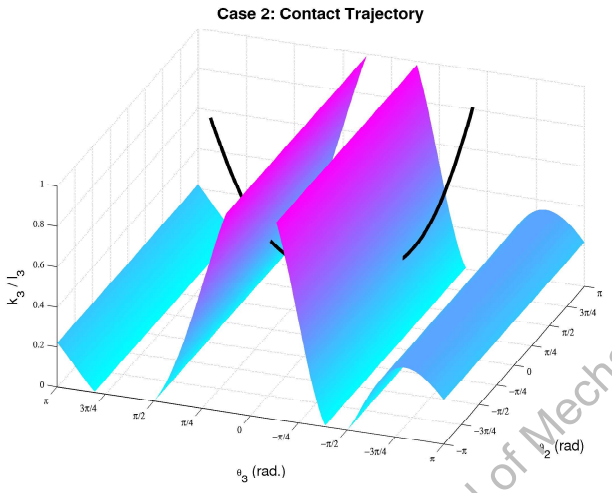

Fig. 10: Grasp-state trajectory and equilibrium surface for the same initial configuration as Fig. 9 - parameter set 1.

rium, or to ejection ($k_3 > l_3$). The expression of the equilibrium surface, defined by $f_2 = 0$, can be explicitly obtained and simplified—by taking into account only the part that can change sign—to

$$\begin{cases} h_2(h_3 \cos\theta_3 - k_3) = 0 & \text{using linkages} \\ (r_3 - r_4)k_3 - r_4 l_2 \cos\theta_3 = 0 & \text{using tendons.} \end{cases} \tag{20}$$

Note that the surface defined by $h_2 = 0$ has not been plotted in Fig. 10 as stated in the introduction of this section since this case corresponds to both an equilibrium position and a singularity in the transmission linkage where points O_1, P_2 and P_1 lie on the same line: in this configuration, both f_2 and f_3 become zero.

Case 3 The third case is the most interesting, since it is both particular to the three-phalanx finger and the most complex of the three cases. Unfortunately, the problem is now of dimension four. Indeed, every time a phalanx is added to the finger, two grasp-state variables should be added (except for the first phalanx as shown in [15]). Hence, two-phalanx fingers require two variables while three-phalanx fingers require **four** variables and n-phalanx fingers lead to $2(n-1)$ variables. Thus, in this case, one cannot visualize contact trajectories and equilibrium surfaces, similarly to the two-phalanx case. The required variables for a three-phalanx finger are $(k_2, k_3, \theta_2, \theta_3)$. Note that in Case 2, k_2 did not appear, leading to a simplified three-dimensional problem. However, by carefully studying the equations defining the grasp behaviour, a solution can be found to get some insight into this problem. First, consider the equations defining the contact trajectories:

$$d_{oc_2}^2 = l_1^2 + k_2^2 + 2l_1 k_2 \cos\theta_2 \tag{21}$$

$$d_{c_2c_3}^2 = (l_2 - k_2)^2 + k_3^2 + 2(l_2 - k_2)k_3 \cos\theta_3 \tag{22}$$

$$\begin{aligned} d_{oc_3}^2 = {} & 2(l_1 + m_1)(k_3 + m_2)\cos(\theta_2 + \theta_3) \\ & + (l_1 + m_1)^2 + (k_3 + m_2)^2 \end{aligned} \tag{23}$$

where d_{oc_2}, $d_{c_2c_3}$, and d_{oc_3} are respectively the distances between the points $O_1 - C_2$, $C_2 - C_3$, and $O_1 - C_3$ (shown in Fig. 5). These quantities are therefore constant, since the object is assumed to be fixed in space. Terms m_1 and m_2 are short notations for:

$$\begin{cases} m_1 = m \sin\theta_3 \\ m_2 = m \sin\theta_2 \end{cases} \quad \text{with } m = \frac{l_2 \sin(\theta_3 - \theta_2)}{\cos^2\theta_2 - \cos^2\theta_3} \tag{24}$$

The equilibrium surface is defined as $U(\theta_2, \theta_3, k_2, k_3) = 0$, where U is the part of f_1 that can change sign, similarly to Case 2. For example, with a tendon-driven finger, one obtains:

$$\begin{aligned} U = {} & l_1 r_2 \cos\theta_2 (r_4 l_2 \cos\theta_3 + (r_4 - r_3)k_3) + \\ & k_2 k_3 r_3 (r_1 - r_2) - l_1 r_2 r_4 k_2 \cos(\theta_2 + \theta_3) \end{aligned} \tag{25}$$

And for a linkage-driven finger:

$$\begin{aligned} U = {} & -h_2 h_3 k_2 \cos(\theta_2 + \theta_3) + k_2 k_3 (h_3 + l_2) \\ & + h_2 l_2 \cos\theta_2 (h_3 \cos\theta_3 - k_3) \end{aligned} \tag{26}$$

where h_2 and h_3 are complex functions of the configuration defined in eq. (6). First, one should note that in this form, the problem is decoupled. The first three equations, namely eqs. (21) to (23) depend only on the contact point locations while the last one, eq. (25) or (26), depends only on the transmission used. Now, one has four equations with four variables, the equilibrium locus being a hypersurface in the grasp-state space. However, visualization can be achieved by writing the three contact equations in a certain form, namely, the form presented in eqs. (21) to (23). Indeed, there are numerous ways of writing the contact equations but only this one has been found interesting. By looking closely at eq. (21), it is observed that a one-to-one relationship is easily obtained from this equation between θ_2 and k_2, provided that an estimated k_2 can be evaluated to choose one of the two solutions of this equation (for a known θ_2), namely

$$k_2 = -l_1 \cos\theta_2 + \delta \sqrt{d_{oc_2}^2 - l_1^2 \sin^2\theta_2} \tag{27}$$

with $\delta = \pm 1$. The solution corresponding to $0 < k_2 < l_2$ must be chosen or, when both solutions meet this requirement,

the solution closest to the preceding point on the contact trajectory should be used. This one-to-one relationship can be substituted into the three remaining equations, leading to a system of three equations and three variables that can be visualized in the resulting three-dimensional space, namely $(\theta_2, \theta_3, k_3)$. It is pointed out that this space is the same state space as the one used in Case 2. This "reduced" grasp-state space is similar to the grasp-state plane (θ_2, k_2) for a two-phalanx finger and allows to visualize contact trajectories as well as equilibrium and validation surfaces, and therefore can help to study the grasp stability of the fingers. As a result, to accurately describe the grasp-state trajectory, one does not require k_2, even in Case 3, where it actually exists and changes during the grasp sliding motion. This result was not intuitively expected.

Examples of an equilibrium surface and a grasp-state trajectory are respectively presented in Figs. 11 and 12. Due to the complexity of the surface and the trajectory, they have been plotted separately for legibility purpose.

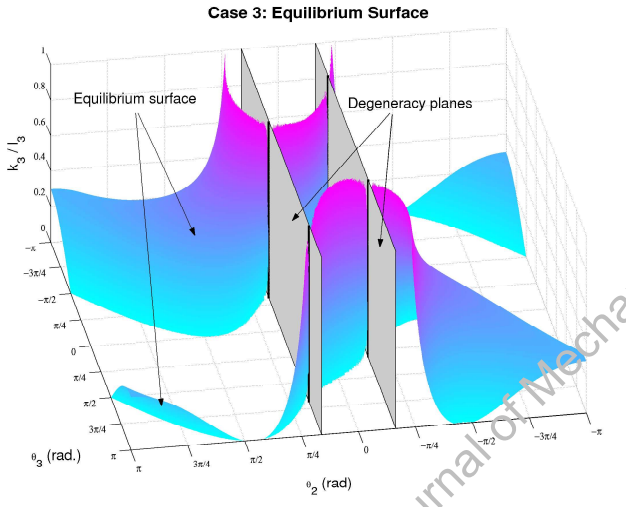

Fig. 11: Case 3: example of equilibrium surface with initial configuration $(\theta_{2i}, \theta_{3i}, k_{2i}, k_{3i}) = (10°, 70°, 0.33, 0.31)$ - parameter set 2.

It is also noted that the words "system of equations" and "variables" have been used rather than "unknowns" since it is not interesting to know if an intersection of the contact trajectory and the equilibrium surface exists. Indeed, a stable configuration can be achieved by attaining a joint limit, so an intersection is not required. Also, to achieve a stable grasp, the contact situation must converge toward the equilibrium locus, which does not always occur. Indeed, convergence to the equilibrium locus depends on the direction in which the contact state is traveling on the contact trajectory, so having an intersection is not sufficient. Thus, a real solution of this system is neither a sufficient nor a necessary condition for a stable grasp. One may wonder how a four-dimensional problem can be reduced to three dimensions. The answer is that the problem is *still* four-dimensional, but we used a property of our system of equations to obtain a graphical

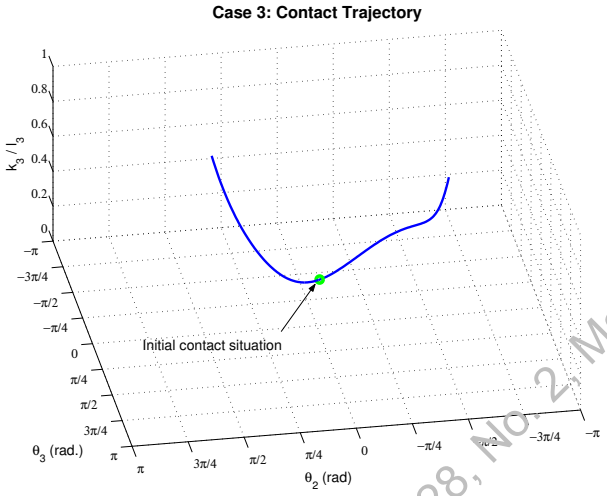

Fig. 12: Case 3: state trajectory with initial configuration $(\theta_{2i}, \theta_{3i}, k_{2i}, k_{3i}) = (10°, 70°, 0.33, 0.31)$ - parameter set 2.

visualisation. Figs. 11 and 12 are indeed neither a projection, nor a section of this four-dimensional space. However, the equilibrium surface for -*this*- trajectory was drawn, which is obtained by substituting the solution of eq. (21) into the equilibrium equation. For other trajectories, i.e., for other initial configurations in the $(\theta_2, \theta_3, k_3)$ space, the equilibrium surface even with the same finger will change, as illustrated in Figs. 13(a) and 13(b). Therefore, with this technique to allow visualization, one looses the decoupling of the problem initially present since now, the equilibrium surface is no longer only function of the geometric configuration and architectural design parameters but also of the initial contact location on the phalanges, an acceptable tradeoff in order to obtain clear and complete visualization.

3.2 Degeneracy Analysis In Fig. 11, two planes have been referred to as degeneracy planes. These planes correspond to a degeneracy in the equilibrium location, i.e. a situation where the equation $U(\theta_2, \theta_3, k_2, k_3) = 0$ is satisfied with k_3 going to infinity, i.e. $k_3(U = 0) = \pm\infty$. These conditions have been previously referred to, for a two-phalanx finger, as degeneracy conditions. Indeed, if the grasp-state of the finger corresponds to one of the latter configurations, the contact location on the distal phalanx leading to a static equilibrium, is pushed to infinity. The degeneracy itself can be either local, i.e. for a particular configuration of the finger (angles θ_2 and θ_3), or global, i.e. for all the finger's configuration. This condition can be easily expressed analytically from eq. (25), for fingers using tendons:

$$k_2 r_3 (r_1 - r_2) + r_2 (r_4 - r_3) l_1 \cos\theta_2 = 0 \qquad (28)$$

Since k_2 and θ_2 are also associated with eq. (21), one can solve this equation to obtain the angle θ_2 corresponding to these planes and examine them in the reduced grasp-state space along with the equilibrium surface. For linkage-driven fingers, the Case 3 degeneracy condition yields to

$$k_2 (h_3 + l_2) - h_2 l_2 \cos\theta_2 = 0 \qquad (29)$$

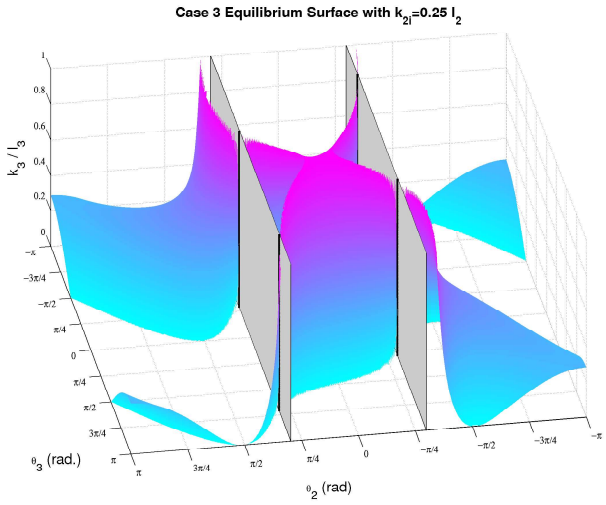

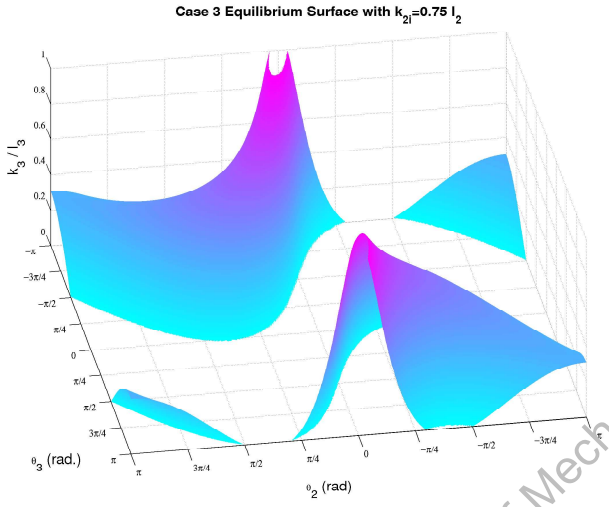

Fig. 13: Equilibrium surfaces with different initial values of k_2 (other parameters are unchanged from Fig. 11).

Similarly, one can use eq. (21) to obtain the angle θ_2 corresponding to a degeneracy configuration. However, one should remember that h_2 and h_3 are complex functions of θ_2 and θ_3. Therefore, one does not have degeneracy planes but rather degeneracy surfaces since these configurations are now also function of θ_3. Nevertheless, the expression of these surfaces can be obtained analytically considering eqs. (6) and (7). An example of case 3 degeneracy locus is presented in Fig. 14 for a linkage-driven finger, the solid curves represent the degeneracy locus as presented in eq. (29) and the dashed curves represent the locus of points where the degeneracy condition creates a paradoxical equilibrium, namely when

$$h_2 h_3 (k_2 \cos(\theta_2 + \theta_3) - l_2 \cos\theta_2 \cos\theta_3) = 0 \qquad (30)$$

Indeed, a subset of these degenerate configurations contradicts the unstable behaviour and leads to a paradoxical equilibrium. If the coefficient in the equilibrium equation U that does not depend on k_3 is also zero, *-any-* contact location leads to static equilibrium. This condition is defined by

$$l_2 \cos\theta_2 \cos\theta_3 - k_2 \cos(\theta_2 + \theta_3) = 0 \qquad (31)$$

for a tendon-driven finger, a result very similar to eq. (30). Therefore, to define these equilibrium configurations, one must solve a set of two trigonometric nonlinear equations—the coefficient of k_3 and the other term in U both equal to zero—for two unknowns (θ_2 and θ_3) using eq. (21). In these peculiar configurations, the equilibrium surface degenerates into two parallel straight lines. In Fig. 11, the four solutions (two solutions for θ_2 and for each one of the latter, two solutions for θ_3) of these equations have been outlined in black. The two curves in Fig. 14 seem to coincide locally (for approx. $\theta_2 = 0$ and $\theta_3 = -\pi/2$) but in fact they do not, the two curves rather intersect in many points in this region of the (θ_2, θ_3) space. The latter intersections correspond to paradoxical equilibrium configurations while there is no equilibrium possible between them, a peculiar behaviour.

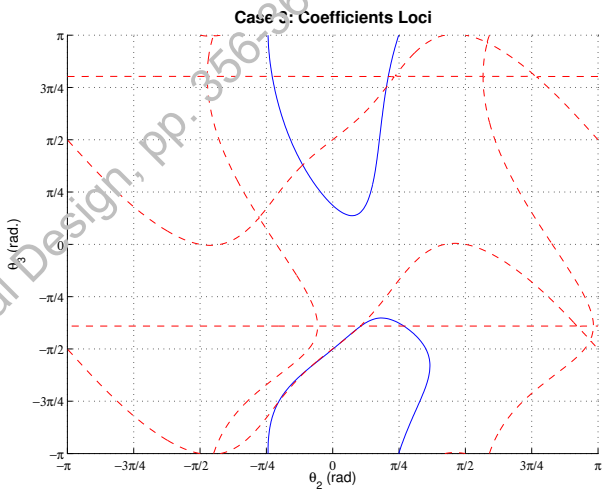

Fig. 14: Case 3 degeneracy analysis.

The inspection of eq. (28) allows to obtain the condition for global (or architectural) degenerated design: $r_1 = r_2$ and $r_3 = r_4$ (assuming $r_i > 0$) for tendon-driven fingers, which is also a sufficient condition for an architectural global Case 2 degeneracy! Indeed, such degeneracies can also happen in Case 2, but the conditions are simpler. Using eq. (20), one obtains

$$\begin{cases} h_3(\theta_3) = \pm\infty & \text{using linkages} \\ r_3 = r_4 & \text{using tendons} \end{cases} \qquad (32)$$

Hence, with Case 2 and for tendon-actuated fingers, no local degeneracy is possible, only a global unstable design, defined with $r_3 = r_4$. The Case 2 degeneracy condition for linkage-driven fingers can be reduced to

$$\cot\beta_2 = \pm\infty \qquad (33)$$

Since $\cot\beta_2$ can be fractionally expressed [15], equating its denominator to zero yields

$$(c_2 \cos(\theta_3 - \psi) + l_2)\sqrt{4a_2^2 b_2^2 - N^2} = M c_2 \sin(\theta_3 - \psi) \qquad (34)$$

with

$$M = -l_2(l_2 + 2c_2\cos(\theta_3 - \psi)) + a_2^2 - b_2^2 - c_2^2$$
$$N = l_2(l_2 + 2c_2\cos(\theta_3 - \psi)) - a_2^2 - b_2^2 + c_2^2$$

Hence, one has the Case 2 degeneracy condition for linkage-driven fingers. By inspection of the degeneracy condition of eq. (34), one can solve the latter equation to obtain the angle θ_3 corresponding to an impossible static equilibrium. Therefore, the Case 2 degeneracy surfaces are in fact, degeneracy planes but with θ_3 constant (as opposed to planes with θ_2 constant in the Case 3 degeneracy condition for tendon transmission).

To summarize, the Case 2 and 3 equilibrium equations have the form:

$$U = f(k_2, \theta_2, \theta_3)k_3 + g(k_2, \theta_2, \theta_3). \tag{35}$$

The degeneracy condition corresponding to an impossible infinite value of the contact location on the distal phalanx is defined as

$$f(k_2, \theta_2, \theta_3) = 0 \tag{36}$$

while the paradoxical equilibrium condition is a subset of the solutions of the latter equation and described by

$$f(k_2, \theta_2, \theta_3) = 0 \quad \text{and} \quad g(k_2, \theta_2, \theta_3) = 0 \tag{37}$$

which lead to an equilibrium for any contact location. The contact location on the distal phalanx has been used in the factoring because it is the evolution of this variable that can lead to ejection. The contact trajectories themselves are not affected by the crossing of a degeneracy surface but no equilibrium is possible in these configurations, except the paradoxical equilibrium previously discussed and defined by eqs. (30) or (31). Since, close to these surfaces, the equilibrium location value increases very quickly to infinity, most of the configurations around these surfaces correspond to a very large value of the equilibrium position and are usually not physically achievable. In conclusion, these configurations are either undesirable (equilibrium point pushed to infinity, often) or ideal (any location leads to equilibrium, rare), but most certainly lead to a peculiar behaviour.

3.3 On the validation surfaces The previous analyses relied on the assumption that during the sliding motion along the contact trajectories, the positive contact forces of the finger do not change sign. This hypothesis is not always satisfied since during the sliding motion of the phalanges on the object, one supplementary contact may be lost. The vanishing of the distal contact force f_3 can be dismissed as contradicting the closing motion of the finger. However, both intermediate and proximal contact forces may be negative, since there is no provision to prevent them from changing sign in the above quasi-static analysis. To completely characterize the grasp-state space, the surface separating the valid part of the latter space from the invalid region—the one in which some contact forces are negative—should be determined. This validation surface can be expressed as $f_1 = 0$ for Case 2 and $f_2 = 0$ for Case 3. Since, in this case the sign of the force is required during the sliding motion, only a dynamic model of the finger can theoretically determine this surface. However, under the hypothesis of a sliding motion relatively slow, which should be the case in many practical applications, especially due to friction, this dynamic behaviour can be approximated [17].

3.4 Loss of two contacts In the case where two contacts are lost ($i = 2$), i.e. in the invalid part defined by the validation surface, the internal mobility of the finger is increased to 2-DOF. Hence, the contact situation evolves not along a contact trajectory but on a contact surface. If, as proposed in this paper the distal phalanx force is assumed to remain positive in all configurations, this situation can only mean that the proximal and intermediate contacts are lost. The contact surface is therefore described by eq. (23). However, the exact contact evolution on the surface itself is unknown since the latter is dependent on the dynamics of the finger. Indeed, with two DOF and one actuator, the general theory of underactuation should now be used to describe the system's state. This time, a quasi-static technique cannot be used to obtain the grasp-state trajectory as in Section 3.3 since the system has 2-DOF. This particular situation is actually a connection between the concept of underactuation in robotic fingers and the theory of underactuation as used in robotics and commonly addressed in the literature. The equilibrium surface can also be described as

$$\begin{cases} f_1 = 0 \\ f_2 = 0 \end{cases} \tag{38}$$

Therefore f_1 depends on k_2, which does not exist. Hence by extrapolating the limit case when both forces are on the edge of vanishing, to evaluate the condition $f_1 = 0$ in terms of the grasp-state variables (θ_2, k_3 and θ_3) one has to ensure that $f_1 = 0$ is actually true for any contact location k_2. One has to decompose f_1 into two separate terms, namely

$$f_1 = a + b/k_2 \tag{39}$$

Then, both a and b are set to zero. It can also be proven that if $b = 0$ then either $f_2 = 0$ or $\cos\theta_2 = 0$, hence the condition for f_2 to become zero is "embedded" in the condition on f_1 (proof not included due to lack of space). Hence, one has to satisfy

$$\begin{cases} a' = (r_1 - r2)r_3k_3 - l_1r_2r_4\cos(\theta_2 + \theta_3) = 0 \\ b' = (r_4 - r_3)k_3 + r_4l_2\cos\theta_3 = 0 \text{ or } \cos\theta_2 = 0 \end{cases} \tag{40}$$

with tendon-driven fingers or

$$\begin{cases} a' = k_3(h_3 + l_2) - h_2h_3\cos(\theta_2 + \theta_3) = 0 \\ b' = k_3 - h_3\cos\theta_3 = 0 \text{ or } \cos\theta_2 = 0 \end{cases} \tag{41}$$

with linkage-driven fingers, where a' and b' are respectively the part of a and b that can become zero ($\cos\theta_2$ has been disregarded for b' to simplify the expressions). Hence, the equilibrium surface is defined by a set of two equations and three variables. It is therefore no longer an equilibrium surface but an equilibrium curve! The latter corresponds to the intersection of the equilibrium conditions for Case 2 and Case 3. As an implication, an equilibrium with contact only on the distal phalanx (without the help of a mechanical limit) is very

rare. It should also be noted that a contact situation leading to the loss of two contacts is quite rare in the usual range of motion of the fingers. For instance, still using the parameters presented in Table 1, the occurences of negative contact forces (implying a loss of contact) over a workspace defined by $0 < \theta_i < \pi/2,\ i = 2,3$ and $0 < k_i < l_i,\ i = 2,3$ are presented in Table 2. As it can be seen and for these two examples, there are no situations leading to the loss of two contacts in the given workspace, also, the most common one contact loss is Case 2.

Table 2: *Percentage of the contact loss occurences*

Parameter set	1	2
3 negative forces	0%	0%
2 negative forces	0%	0%
1 negative force	67.34%	58.79%
- proximal	8.84%	9.13%
- intermediate	58.50%	49.66%
- distal	0%	0%
0 negative force	32.66%	41.21%

3.5 Design Analysis The analyses presented in Sections 3.1 and 3.2 allow one to obtain the final stability of a grasp with respect to an initial configuration of the finger. For instance, if in this initial configuration, one force is negative, one may proceed with the study on the sliding motion of the finger to determine if a stable grasp will be achieved, if the latter uses the mechanical limits of the finger or not, or if the finger will eject the object. This technique can therefore be useful in the design of an underactuated finger that must grasp a certain set of typical objects. One may study the robustness of the finger stability with respect to design parameters, as illustrated in Fig. 15. In this figure, an underactuated finger using tendons is grasping an object with an initial configuration given by $(\theta_2, \theta_3, k_2, k_3) = (\pi/6, \pi/3, 0.5, 0.5)$, i.e. with a missing proximal contact, and the final stability of the grasp is presented with respect to the ratio of the transmission pulley radii. The phalanx lengths used are the same as in parameter set 2, and the full range of both angle, namely $-\pi < \theta_i < \pi$ with $i = 2,3$ has been used.

In this figure, one can identify two distinct regions corresponding to an unstable grasp leading to ejection. The leftmost ejection region corresponds to what has been defined as opening-ejection [14]. The rightmost ejection region corresponds to closing-ejection, a more insidious case of ejection [14] since this phenomenon can happen in the usual range of motion of the joint angles. The same technique can be used with a Case 1 grasp but the illustration is of less importance since in this case the final stability depends only on the ratio r_4/r_3, the first stage of the finger being immobile.

4 Conclusions

In this paper, the grasp stability of two types of three-phalanx underactuated fingers with either linkages or tendons and pulleys, has been discussed. A method to obtain the condition for these fingers to be in equilibrium or to eject the object as well as the equations of the contact trajectories defining the motion undergone by the finger when one or more contacts are missing on the phalanges, was discussed. This work is only the first step towards a more general grasp stability theory. Indeed, the model presented here could be refined to include friction, local contact geometries, spring stiffnesses, if these characteristics are required for an accurate modeling. The grasp stability remains to be fully determined in the case where two contacts are lost, showing the limit of our approach that does not use a dynamic modeling. Furthermore, the assumption on the initial configuration, namely that initially the finger closed all phalanges on the object as illustrated in Fig. 2*i*, does not necessarily hold since during the closing process, contact with the first phalanges could be lost. This again illustrates the need to obtain a stability theory taking into account all contact situations, i.e. establishing the contact dynamics of the finger.

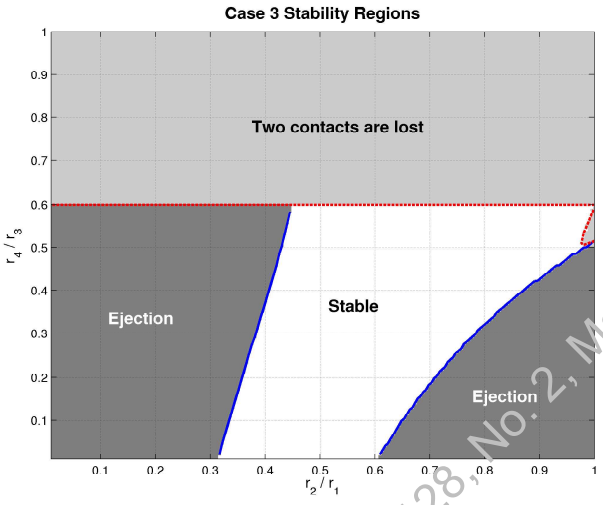

Fig. 15: Case 3 stability regions with respect to design parameters.

Acknowledgments

The financial support of the Natural Sciences and Engineering Research Council of Canada (NSERC) and the Canada Research Chair Program is acknowledged.

References

[1] Jacobsen, S. C., Iversen, E. K., Knutti, D. F., Johnson, R. T., and Biggers, K. B., 1986, "Design of the Utah/MIT Dextrous Hand," Proc. of the 1986 IEEE Intl. Conf. Rob. Aut., San Francisco, CA, pp. 1520-1532.

[2] Salisbury, J. K., and Craig, J. J., 1982, "Articulated Hands: Force Control and Kinematic Issues," Intl. J. Rob. Res., **1**(1), pp. 4-17.

[3] Butterfass, J., Grebenstein, M., Liu, H., and Hirzinger, G., 2001, "DLR-Hand II: Next Generation of a Dextrous Robot Hand," Proc. IEEE Intl. Conf. Rob. Aut., Seoul, Korea, pp. 109-114.

[4] Okada, T., 1982, "Computer Control of Multijointed Finger System for Precise Object-Handling," IEEE Trans. Sys. Man Cyb., **12**(3), pp. 289-299.

[5] Bicchi, A., and Kumar, V., 2000, "Robotic Grasping and Contact: A Review," Proc. IEEE Intl. Conf. Rob. Aut., San Francisco, CA, pp. 348-353.

[6] Akin, D. L., Carignan, C. R., and Foster, A. W., 2002, "Development of a Four-Fingered Dexterous Robot End Effector For Space Operations," Proc. IEEE Intl. Conf. Rob. Aut., Washington, DC, pp. 2302-2308.

[7] Biagiotti, L., Melchiorri, C., and Vassura, G., 2001, "Control of a Robotic Gripper for Grasping Objects in No-Gravity Conditions," Proc. IEEE Intl. Conf. Rob. and Aut., Seoul, Korea, pp. 1427-1432.

[8] Figliolini, G., and Ceccarelli, M., 2002, "A Novel Articulated Mechanism Mimicking the Motion of Index Fingers," Robotica, **20**(1), pp. 13-22.

[9] Rakic, M., 1989, "Multifingered Robot Hand With Self-Adaptability," Rob. Comp.-integ. Manuf., **3**(2), pp. 269-276.

[10] Hirose, S., and Umetani, Y., 1978, "The Development of Soft Gripper for the Versatile Robot Hand," Mech. Mach. Th., **13**, pp. 351-358.

[11] Laliberté, T., and Gosselin, C., 1998, "Simulation and Design of Underactuated Mechanical Hands," Mech. Mach. Th., **33**(1), pp. 39-57.

[12] Carrozza, M. C., Vecchi, F., Sebastiani, F., Cappiello, G., Roccella, S., Zecca, M., Lazzarini, R., and Dario, P., 2003, "Experimental Analysis of an Innovative Prosthetic Hand with Proprioceptive Sensors," Proc. IEEE Intl. Conf. Rob. Aut., Taipei, Taiwan, pp. 2230-2235.

[13] Herder, J. L., and de Visser, H., 2000, "Force Directed Design of a Voluntary Closing Hand Prosthesis," Proc. ASME Des. Eng. Tech. Conf., Baltimore, MD, pp. 1-8.

[14] Birglen, L., and Gosselin, C., 2003, "On the Force Capabilities of Underactuated Fingers," Proc. IEEE Intl. Conf. Rob. Aut., Taipei, Taiwan, pp. 1139-1145.

[15] Birglen, L., and Gosselin, C., 2004, "Kinetostatic Analysis of Underactuated Fingers," IEEE Trans. Rob. Aut., **20**(2), pp. 211-221.

[16] Birglen, L., and Gosselin, C., 2004, "Optimal Design of 2-Phalanx Underactuated Fingers," Proc. Intl. Conf. Intel. Manip. Grasp., Genova, Italy, pp. 110-116.

[17] Birglen, L., 2004, "Analysis and Control of Underactuated Robotic Hands," Ph.D. Thesis, Faculté des sciences et de génie, Université Laval, Québec, Canada.